

# Identification and validation of necroptosis-related gene signatures to predict clinical outcomes and therapeutic responses in acute myeloid leukemia

Xiang-Mei Wen<sup>1,2,3,\*</sup>, Zi-Jun Xu<sup>1,2,3,\*</sup>, Ji-Chun Ma<sup>1,2,3</sup>, Pei-Hui Xia<sup>1,2,3</sup>, Ye Jin<sup>2,4</sup>, Xin-Yi Chen<sup>1,2,3</sup>, Wei Qian<sup>5,&</sup>, Jiang Lin<sup>1,2,3,&</sup>, Jun Qian<sup>2,4</sup>

<sup>1</sup>Laboratory Center, Affiliated People's Hospital of Jiangsu University, Zhenjiang 212002, Jiangsu, P.R. China

<sup>2</sup>Zhenjiang Clinical Research Center of Hematology, Affiliated People's Hospital of Jiangsu University, Zhenjiang 212002, Jiangsu, P.R. China

<sup>3</sup>The Key Lab of Precision Diagnosis and Treatment in Hematologic Malignancies of Zhenjiang City, Affiliated People's Hospital of Jiangsu University, Zhenjiang 212002, Jiangsu, P.R. China

<sup>4</sup>Department of Hematology, Affiliated People's Hospital of Jiangsu University, Zhenjiang 212002, Jiangsu, P.R. China

<sup>5</sup>Department of Otolaryngology-Head and Neck Surgery, Affiliated People's Hospital of Jiangsu University, Zhenjiang 212002, Jiangsu, P.R. China

\*Equal contribution

**Correspondence to:** Jun Qian, Jiang Lin, Wei Qian; email: [qianjun@ujs.edu.cn](mailto:qianjun@ujs.edu.cn); [2651329493@qq.com](mailto:2651329493@qq.com), <https://orcid.org/0000-0002-4704-9157>; [dwqian@yahoo.com](mailto:dwqian@yahoo.com), <https://orcid.org/0009-0001-9729-1902>

**Keywords:** necroptosis, acute myeloid leukemia, prognosis, tumor microenvironment, immune infiltration, immunotherapy

**Received:** May 15, 2023

**Accepted:** October 2, 2023

**Published:** November 21, 2023

**Copyright:** © 2023 Wen et al. This is an open access article distributed under the terms of the [Creative Commons Attribution License](https://creativecommons.org/licenses/by/4.0/) (CC BY 4.0), which permits unrestricted use, distribution, and reproduction in any medium, provided the original author and source are credited.

## ABSTRACT

**Background:** Necroptosis is a tightly regulated form of necrotic cell death that promotes inflammation and contributes to disease development. However, the potential roles of necroptosis-related genes (NRGs) in acute myeloid leukemia (AML) have not been elucidated fully.

**Methods:** We conducted a study to identify a robust biomarker signature for predicting the prognosis and immunotherapy efficacy based on NRGs in AML. We analyzed the genetic and transcriptional alterations of NRGs in 151 patients with AML. Then, we identified three necroptosis clusters. Moreover, a necroptosis score was constructed and assessed based on the differentially expressed genes (DEGs) between the three necroptosis clusters.

**Results:** Three necroptosis clusters were correlated with clinical characteristics, prognosis, the tumor microenvironment, and infiltration of immune cells. A high necroptosis score was positively associated with a poor prognosis, immune-cell infiltration, expression of programmed cell death 1/programmed cell death ligand 1 (PD-1/PD-L1), immune score, stromal score, interferon-gamma (IFNG), merck18, T-cell dysfunction-score signatures, and cluster of differentiation-86, but negatively correlated with tumor immune dysfunction and exclusion score, myeloid-derived suppressor cells, and M2-type tumor-associated macrophages. Our observations indicated that a high necroptosis score might contribute to immune evasion. More interestingly, AML patients with a high necroptosis score may benefit from treatment based on immune checkpoint blockade.

**Conclusions:** Consequently, our findings may contribute to deeper understanding of NRGs in AML, and facilitate assessment of the prognosis and treatment strategies.

## INTRODUCTION

Acute myeloid leukemia (AML) is a highly lethal hematological malignancy. It is characterized by proliferative enhancement, blocked differentiation, and dysregulated apoptosis [1]. Intensive induction chemotherapy is first-line treatment for AML [2]. Conventional types of chemotherapy can induce remission in some patients, but most patients experience a relapse of AML [3]. For decades, many novel targeted therapies have been developed, but the prognosis for AML remains poor, with 5-year survival of ~10% [4, 5]. Also, childhood AML has an unfavorable prognosis, and the prevalence of relapse is high [6]. Therefore, identifying new molecular profiles that can predict the prognosis and aid development of new therapeutic targets against AML is important.

Necroptosis is a type of regulated cell death characterized by loss of plasma-membrane integrity and escape of cellular contents that is independent of caspases, the morphological characteristics of necrosis, and instigation of an inflammatory response [7–10]. The main mediators of necroptosis execution are receptor interacting protein kinase 1 (RIPK1) and RIPK3, and mixed lineage kinase domain-like protein [8, 11]. Recently, several studies have demonstrated the influence of necroptosis on tumorigenesis, progression, and metastasis in various types of cancer [12, 13]. The pro-tumorigenic or antitumorigenic effects of RIPK3-mediated necroptosis are dependent upon the type of cancer and conditions during tumorigenesis. It has been reported that RIPK3 deficiency does not alter MYC-driven lymphomagenesis or the killing of malignant lymphoma cells induced by chemotherapeutics [14]. Moreover, RIPK3 expression is downregulated and correlates with poor clinical outcomes in AML [12, 15]. However, the key mediators of the necroptotic pathway (alone or in combination) have been shown to enhance neoplastic progression and metastasis [16, 17].

Necroptosis is a type of inflammatory cell death that contributes to innate immunity and shapes subsequent adaptive immunity [18, 19]. The machinery of necroptotic cell death promotes immune responses by increasing secretion of cytokines and chemokines [20, 21]. RIPK1 signaling and activation of nuclear factor-kappa B may be necessary during necroptotic cell death to result in efficient cross-priming and antitumor immunity [22]. Nevertheless, necroptotic tumor cells also attract dendritic cells and macrophages that can further enhance immunosuppression [23]. Thus, necroptosis can shape adaptive immunity against tumor progression and generate an immunosuppressive tumor microenvironment (TME).

Due to technical limitations, most studies have investigated only one or two necroptosis-related genes (NRGs). Numerous genes interact with each other and with environmental factors in a highly coordinated manner. The signatures of novel NRGs for the prognosis or TME of hepatocellular carcinoma, colon cancer, bladder cancer, pancreatic cancer, and cutaneous melanoma have been identified [24–28]. However, the prognostic role of the NRG signature in AML has not been elucidated. We explored the association of multiple NRGs with the prognosis of AML and cell infiltration into the TME. We aimed to provide insights into tumorigenesis and open-up a novel therapeutic strategy for AML.

## MATERIALS AND METHODS

### Data acquisition

The raw data of transcriptome profiling and corresponding clinical information of 151 AML samples were downloaded from the Genomic Data Commons of The Cancer Genome Atlas (TCGA) portal (<https://portal.gdc.cancer.gov/repository>). Since normal samples were not included in AML from TCGA database, we collected 70 bone marrow (BM) normal samples from the GTEx database (<http://www.GTExportal.org/home/>). Batch effects between two datasets were corrected using the “ComBat” method from the *sva* package. Detailed information on these AML patients is shown in Supplementary Table 1. Data on the somatic gene mutations and gene copy number variations (CNVs) of AML patients were also obtained from TCGA database. Data on somatic mutations were analyzed with the “mafCompare” function in the “Maftools” package [29]. Significant amplifications or deletions of the copy number were detected by filtered segmented copy number data (Affymetrix SNP 6.0 platform) using the GISTIC2.0 algorithm [30]. We also collected six AML datasets (GSE6891, GSE10358, GSE12417\_UA, GSE12417\_UP, GSE37642\_UA, and GSE37642\_UP), combining them using the “ComBat” algorithm, in order to validate the consensus clustering results in TCGA.

### Consensus molecular clustering for 67 NRGs

A list of NRGs was collected from the work of Zirui Zhao and colleagues [31]. All 67 genes are provided in Supplementary Table 2. We applied the “ConsensusClusterPlus” package for consensus clustering and distinguishing patients into three distinct necroptosis clusters based on these 67 NRGs [32]. Consensus clustering is an established unsupervised classification method for data analyses. The appropriate cluster number (*k*) was calculated from the relative

change in area under the cumulative distribution function. Plots were created to ascertain if they are consistent or inconsistent for various values of  $k$ .

### Identification of differentially expressed genes (DEGs)

DEGs were identified among three necroptosis subtypes via the “limma” package in R 4.0.4 (R Institute for Statistical Computing, Vienna, Austria; <http://www.r-project.org/>). Specifically, with the “limma-voom” package, we normalized gene expression, which was then fed into “lmFit” and “eBayes” functions in the limma package. A total of 829 DEGs were identified. Patients were divided into three gene clusters via unsupervised clustering of DEGs.

### Generation of a necroptosis score

We also used principal component analysis (PCA) to evaluate the necroptosis pattern for each individual. First, univariate Cox regression analysis was undertaken on 829 DEGs to identify prognosis-related genes. Second, we conducted recursive feature elimination with 10-fold cross-validation in the 361 genes that had a significant prognostic impact. Third, we carried out PCA to construct a signature of the relevant genes of necroptosis with principal component (PC)1 and 2 as signature scores. Accordingly, we calculated a necroptosis score [33]:

$$\text{Necroptosis score} = \sum(\text{PC}1i + \text{PC}2i)$$

where  $i$  is the expression of NRGs.

AML patients were divided into a low-score group and high-score group according to the maximally selected rank statistics (maxstat) method.

### Clinical features and analyses of signaling-pathway enrichment

We examined the relationships between different AML subtypes and clinicopathological characteristics, including French–American–British (FAB) subtypes, cytogenetic risk, sex, age, and white blood cell count. To explore biological information and protein functions, enrichment analyses were done with the “clusterprofile” package in R using the Gene Ontology (GO) database (<http://www.geneontology.org/>). We detected significant differences in signaling pathways between different groups using the R package “GSVA”.

### Estimation of infiltration of TME cells and prediction of immune responses

We adopted the CIBERSORT algorithm to quantify infiltration of immune cells in different NRGs patterns

[34]. As part of this analysis, the ESTIMATE algorithm was used to analyze the tumor purity, immune score, and stromal score [35]. We also analyzed the correlations between expression of programmed cell death 1/programmed cell death ligand 1 (PD-1/PD-L1) and the necroptosis score. We collected four independent immunotherapy cohorts including four cancer types to determine difference in immune checkpoint blockade (ICB) responsiveness between patients with high and low necroptosis score. The response information was downloaded from the supplementary data of the respective papers.

### Statistical analyses

R was employed for statistical analyses. Kaplan–Meier survival curves were used to assess survival differences between patient groups using the “survminer” package. Categorical data were compared using the chi-square test or Fisher’s exact test. The correlation between continuous variables was compared using Spearman’s rank correlation test. Data visualization was undertaken using the R packages “ggplot2”, “circlize” (for Circos plots), and Maftools (for co-onco plots or forest plots).  $P < 0.05$  was considered significant.

### Data and code availability

The code files (using R) employed to reproduce the figures contained within the manuscript are available upon reasonable request. The original contributions presented in the study are provided in the Article/Supplementary Materials.

## RESULTS

### “Landscape” of genetic and transcriptional alterations of NRGs in AML

We assessed 67 NRGs (Supplementary Table 1). To reveal chromosomal gains and losses, we applied a somatic CNV analysis. The CNV of NRGs was not prevalent in AML. TRIM11, CYLD, and ID1 were involved primarily in gene amplification, whereas deletion of HSPA4, BRAF, and SQSTM1 was common (Figure 1A, Supplementary Table 2). The location of CNV alteration of 67 NRGs on chromosomes is illustrated in Figure 1B (Supplementary Tables 3, 4). Normal samples and tumor samples could be distinguished clearly into two distinct groups via PCA (Supplementary Figure 1A). Also, the prevalence of somatic mutations of NRGs in AML was not widespread, and the top-eight genes with altered expression were FLT3 (8%), IDH2 (7%), IDH1 (5%), AXL (1%), MYC (1%), DNMT1 (1%), ALK (1%), and SLC39A7 (1%) (Figure 1C). We also compared mRNA



investigate the prognostic value of NRGs (Supplementary Table 6). A consensus clustering analysis based on expression of NRGs was conducted for AML. The optimal  $k$  value was 3 (Supplementary Figure 2A–2C). According to PCA, three clusters had significant differences in their gene-expression profiles (Figure

2A). The entire cohort was clustered into necroptosis cluster A ( $n = 71$ ), necroptosis cluster B ( $n = 36$ ), and necroptosis cluster C ( $n = 44$ ) (Figure 2B). Kaplan–Meier survival curves for overall survival (OS) indicated significant differences among the three clusters. Patients with necroptosis cluster B had a poor

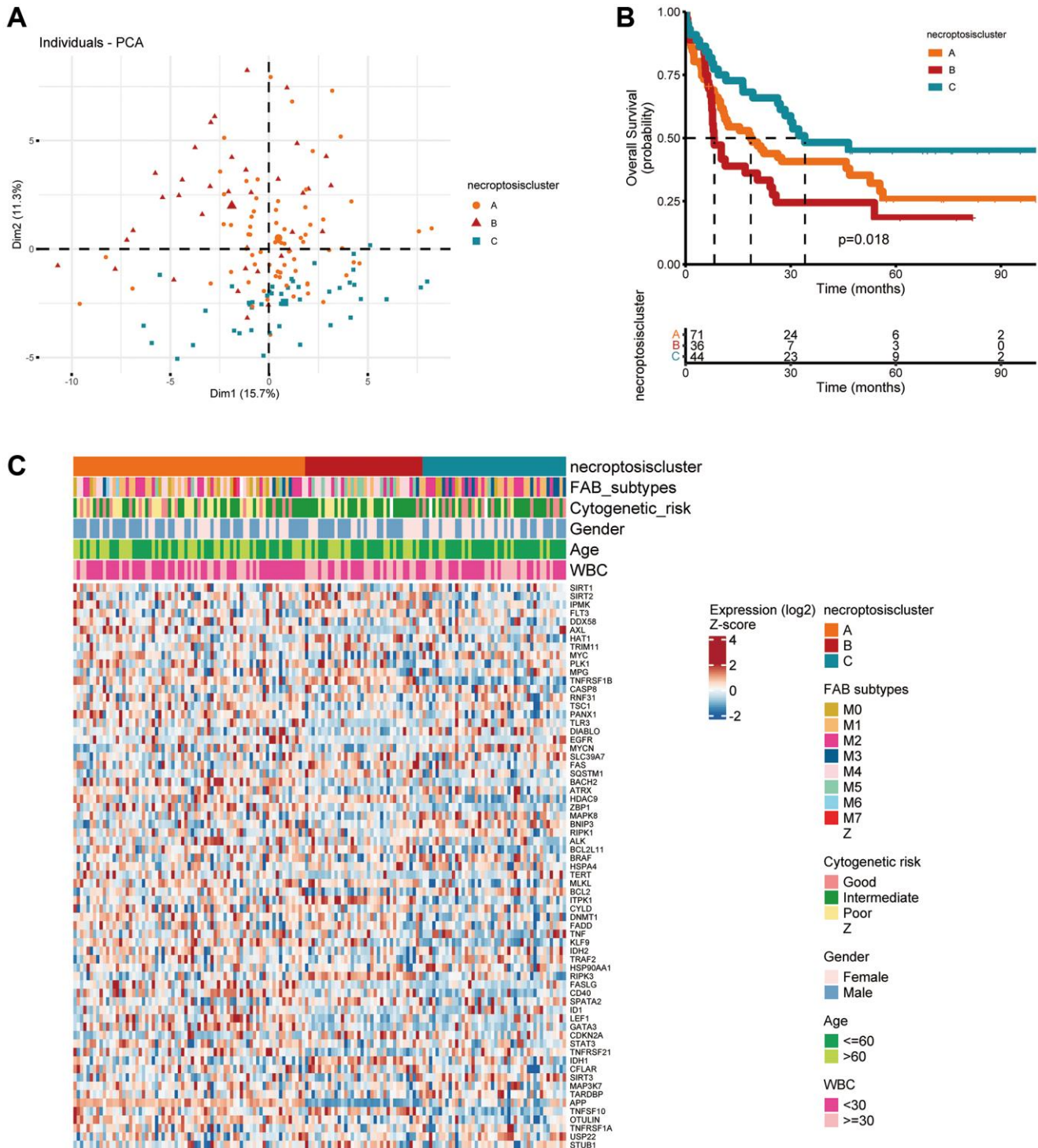


**Figure 2. Subtypes of necroptosis-related genes and their clinicopathological and biological characteristics in AML. (A)** PCA of transcriptomes among the three identified clusters. **(B)** Kaplan–Meier curves showing overall survival for the three necroptosis clusters. **(C)** Clinicopathological characteristics and expression of necroptosis-related genes among the three necroptosis clusters.

survival outcome ( $P = 0.018$ ) (Figure 2B). Moreover, the three clusters were confirmed by performing consensus clustering analysis in combined AML cohorts encompassing six datasets (1115 patients), although the prognostic impact was not validated (Supplementary Figure 3). Then, the clinicopathological characteristics of the three necroptosis subtypes were compared. Cases with FAB M3 was mainly observed in patients with necroptosis cluster C. Necroptosis cluster B was not associated with good cytogenetic risk and APP was barely expressed in necroptosis cluster B. In terms of gender, age and WBC, no differences were observed among three clusters (Figure 2C).

### Associations between the TME and three necroptosis clusters

Using the CIBERSORT algorithm, we explored the profiles of 23 types of infiltrating immune cells in three necroptosis clusters. Significant differences in immune-cell infiltration were noted except for cluster of differentiation (CD)56 bright natural killer cells

among the three types of necroptosis clusters (Figure 3A). Necroptosis cluster B had the highest number of infiltrating macrophages. Enrichment analyses using the GSVA package were also done to elucidate the biological characteristics among the three necroptosis clusters. Necroptosis cluster B was strongly related to metabolic pathways, including “phenylalanine metabolism”, “histidine metabolism”, and “sulfur metabolism” (Figure 3B, Supplementary Table 7). Necroptosis cluster A showed significant enrichment in immune system-related pathways such as “systemic lupus erythematosus”, “intestinal immune network for IgA production”, “cell adhesion molecules”, “cytokine receptor interaction”, “T cell receptor signaling pathway”, “natural killer cell-mediated cytotoxicity”, and “chemokine signaling pathway activation” (Figure 3C, Supplementary Table 8). Necroptosis cluster B was also highly associated with immune system-related pathways, including “intestinal immune network for IgA production”, “NOD-like, and Toll-like receptor signaling pathway”, “B cell receptor signaling pathway”, and “natural killer cell-mediated cytotoxicity” (Figure 3D, Supplementary Table 9).

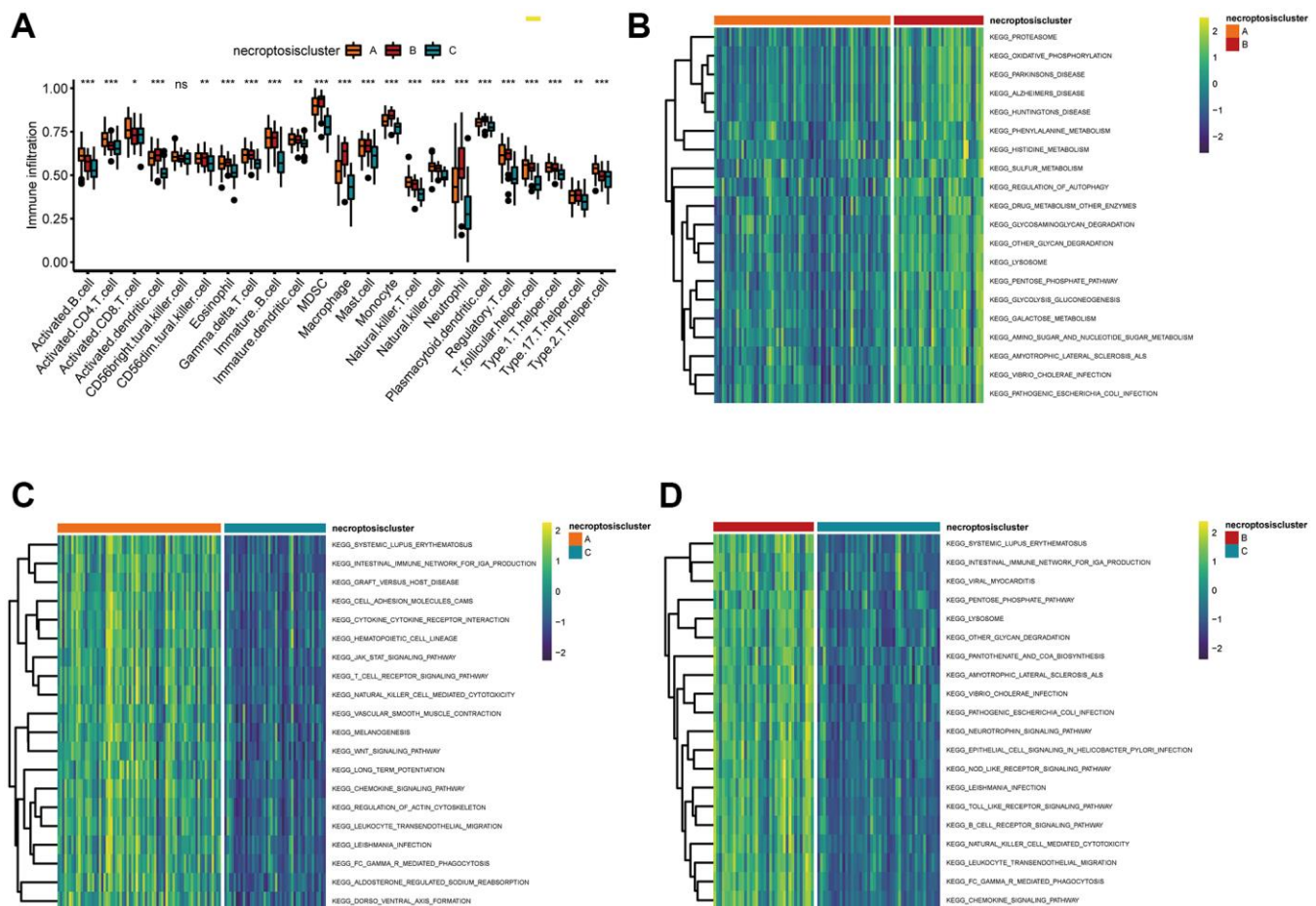


**Figure 3. Correlations between the TME and three necroptosis clusters.** (A) Analyses of tumor-infiltrating immune cells in the three necroptosis clusters. \* $P < 0.05$ , \*\* $P < 0.01$ , \*\*\* $P < 0.001$ , ns, not significant. (B–D) Heatmap of the enrichment analyses in three necroptosis clusters using the GSVA package. (B) Cluster A vs. cluster B; (C), cluster A vs. cluster C; (D), cluster B vs. cluster C.

## Identification of three gene clusters in AML

We wished to further investigate the underlying biological functions of the three clusters. We generated a Venn diagram to illustrate the overlapped DEGs, and a set of 829 genes was screened out (Figure 4A). Subsequently, functional analyses were done using the GO database. Expression of necroptosis subtype-related genes associated with immunity was increased significantly (Figure 4B, Supplementary Table 10), which indicated that necroptosis may participate in regulation of the immune function of the TME. We wished to identify the genes associated with the prognosis among these 829 common DEGs. Hence, we undertook univariate Cox regression analysis and selected 316 genes with  $P < 0.05$  to use in subsequent analyses (Supplementary Table 11). Three gene clusters were identified using consensus clustering, and we named them as gene clusters A, B, and C (Figure 4C).

Kaplan–Meier curves for OS showed that patients with gene cluster A or gene cluster B had a worse outcome than that for patients with gene cluster C ( $P < 0.001$ , log-rank test) (Figure 4D). Moreover, the three gene clusters were confirmed using consensus clustering analysis in combined AML cohorts encompassing six datasets (1115 patients), and the prognostic impact was validated ( $P < 0.001$ , log-rank test) (Supplementary Figure 4A, 4B). Among the three gene clusters, there were significant differences in expression of NRGs such as SIRT1, SIRT2, IPMK, and AXL (Figure 5A). Necroptosis gene cluster C correlated with good cytogenetic risk. More interestingly, these 316 genes showed high expression in gene cluster B (Figure 5B).

## Construction and validation of a necroptosis score

We applied a PCA algorithm to calculate the necroptosis score and quantify necroptosis patterns

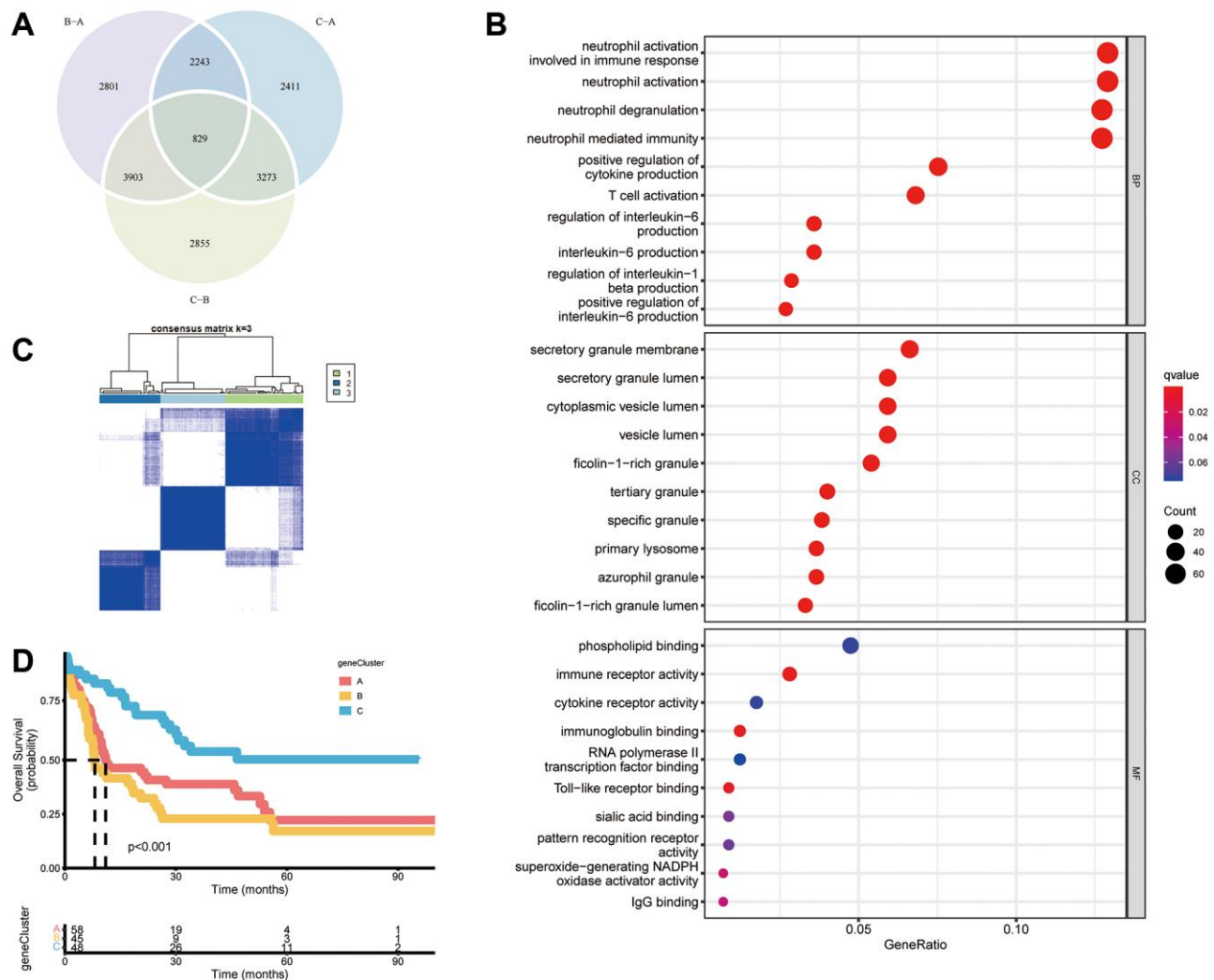


**Figure 4. Construction of gene subtypes based on DEGs.** (A) Venn diagram of 829 necroptosis-related DEGs among three necroptosis clusters. (B) Analyses of functional enrichment of DEGs using the GO database. (C) Three gene clusters were categorized by a consensus matrix heatmap ( $k = 3$ ). (D) Kaplan–Meier curves of overall survival for three gene clusters ( $P < 0.001$ , log-rank test).

among AML patients because of the complexity and individual heterogeneity in necroptosis modification (Supplementary Table 12). The alluvial plot (Figure 6A) illustrated the distribution of the three necroptosis clusters, three necroptosis gene clusters, necroptosis score, and OS status. Cluster B had a higher necroptosis score than that of cluster A or cluster C (Figure 6B). The necroptosis score of gene cluster B was

higher than that of gene cluster A and gene cluster C (Figure 6C). We conducted OS analyses using Kaplan–Meier curves. Patients with a high necroptosis score had a significantly poor prognosis than those with a low necroptosis score ( $P < 0.001$ , log-rank test) (Figure 6D). Furthermore, the prognostic impact was validated in combined AML cohorts encompassing six datasets (1115 patients) ( $P < 0.001$ , log-rank test)

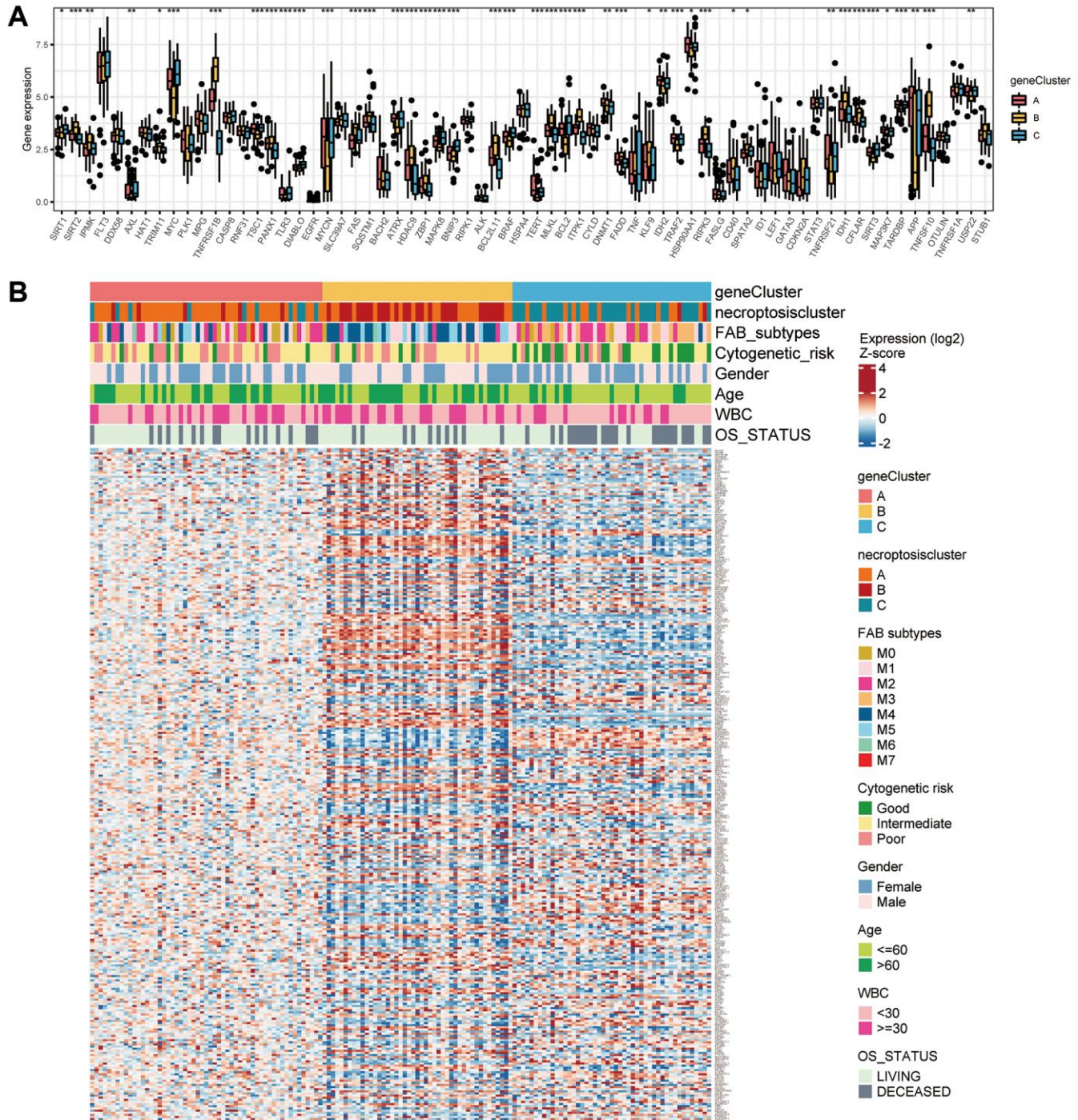


**Figure 5. Correlations between the TME and three gene clusters. (A)** Gene expression of 67 necroptosis-related genes among the three gene clusters. **(B)** Association of clinicopathologic features with the three gene clusters.

(Supplementary Figure 4C). Univariate Cox regression analyses revealed a high necroptosis score to be significantly related to shorter OS (HR = 7.673,  $P < 0.01$ ) (Supplementary Table 13). Multivariate Cox regression analyses for OS in TCGA dataset confirmed the necroptosis score to be an independent prognostic biomarker in AML (HR = 3.792,  $P =$

0.0287) (Figure 6E). We analyzed the most prevalent somatic mutations for a high score and low necroptosis score to study differences in distribution of somatic mutations between them. FLT3 (30% vs. 11%) and DNMT3A (25% vs. 17%) had a higher prevalence of somatic mutations in the group with a high necroptosis score (Figure 6F, 6G).

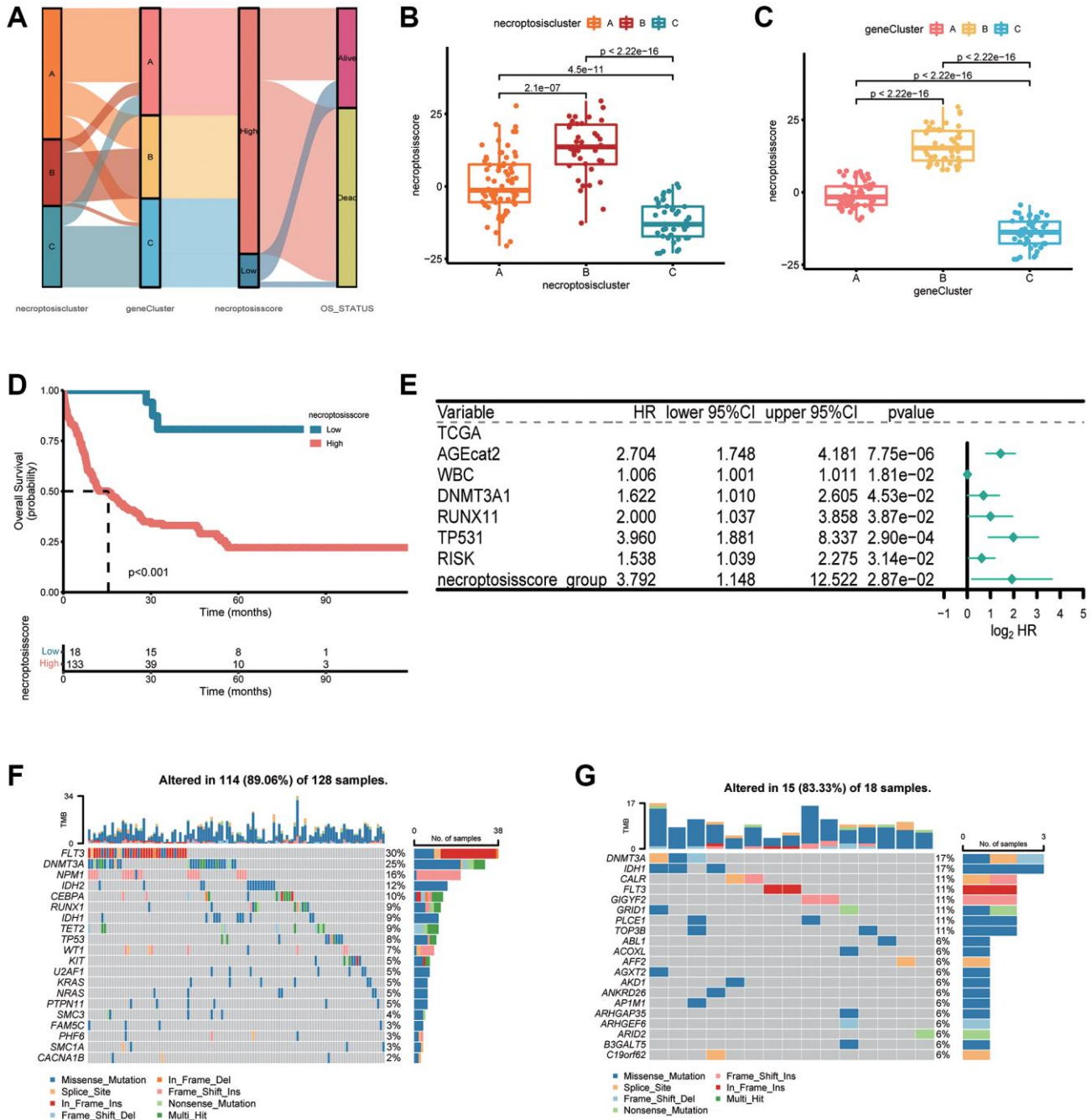


**Figure 6. Construction of a necroptosis score and its clinical relevance.** (A) Alluvial plot depicting subtype distributions in groups with different necroptosis clusters, gene clusters, necroptosis score, and overall survival. (B) Differences in the necroptosis score between three necroptosis clusters. (C) Differences in the necroptosis score between three gene clusters. (D) Kaplan–Meier survival analysis of groups with a high necroptosis score or low necroptosis score ( $P < 0.001$ , log-rank test). (E) Multivariate Cox regression analyses of the overall survival of AML patients. (F, G) “Waterfall” plot of somatic mutation features in groups with the high necroptosis score (F) or low necroptosis score (G).

## Necroptosis score in immunotherapy

Next, we investigated if the necroptosis score could be used to predict the response to immunotherapy by patients. We analyzed the correlation between the

abundance of immune cells and necroptosis score. The number of activated dendritic cells, gamma delta T cells, macrophages, mast cells, and natural killer T cells was positively related to the necroptosis score (Figure 7A and Supplementary Table 14). The group with a high

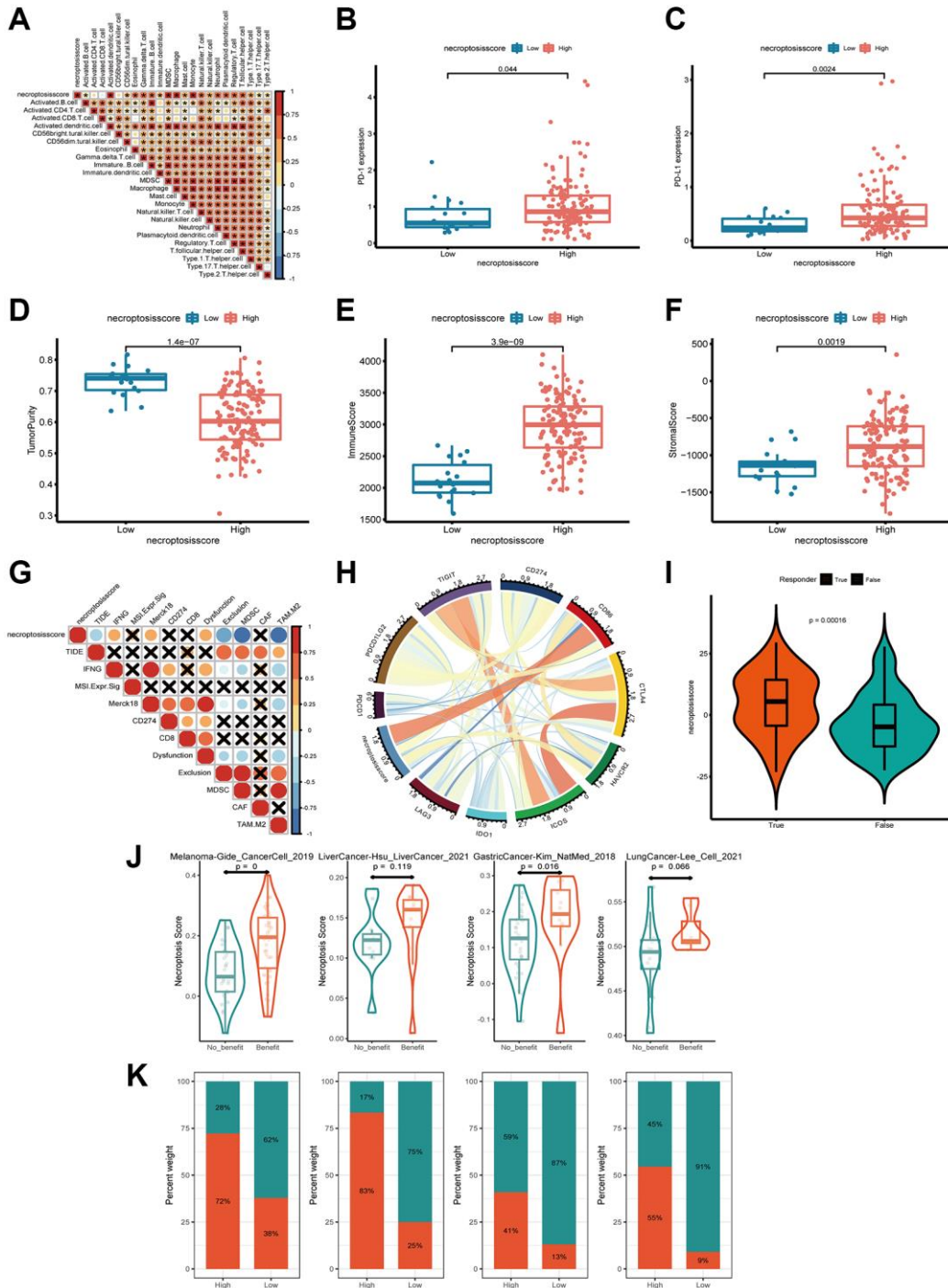


**Figure 7. Exploration of the response of the necroptosis score to immunotherapy.** (A) Spearman correlation analysis of tumor-infiltrating lymphocytes and necroptosis score. (B, C) Expression of PD-L1 and PD-1 in groups with a high necroptosis score (B) and low necroptosis score (C). (D–F) Tumor purity, immune score, and stromal score of necroptosis-score groups were analyzed and plotted. (G, H) Correlations between necroptosis and other immune checkpoints in AML. (I) Profile of the necroptosis score in the non-responder group and responder group. (J, K) Patients with a higher necroptosis score have a higher response to ICB in four independent ICB cohorts comprising of four cancer types.

necroptosis score had upregulated expression of PD-1 and PD-L1, which impaired antitumor immunity further (Figure 7B, 7C).

Based on these findings, we aimed to estimate the overall number of infiltrating immune cells and stromal cells in the groups with a high necroptosis score and low necroptosis score, respectively. We used the ESTIMATE algorithm to calculate tumor purity, immune score, and stromal score. There was a tendency for the group with a high necroptosis score to have lower tumor purity, higher immune score and stromal score (Figure 7D–7F). These data indicated that the group with a high necroptosis score was enclosed by more nontumor components. To identify the group that may be a candidate for immunotherapy, we analyzed the response to immunotherapy based on the necroptosis score. We observed a strong negative correlation between the necroptosis score and T-cell exclusion signatures, including tumor immune dysfunction and exclusion core, myeloid-derived suppressor cells (MDSCs) and the M2 subtype of tumor-associated macrophages (TAMs). The opposite trend was observed among interferon-gamma (IFNG), merck18, and T-cell dysfunction-score signatures (Figure 7G). These findings demonstrated indirectly that the necroptosis score had a critical role in mediating the immune response, and that the group with a high necroptosis score was potentially more sensitive to immunotherapy.

Moreover, we investigated the correlation between the necroptosis score and a collection of genes associated with checkpoints in AML. CD86 was constantly associated with the necroptosis score according to Circos plots (Figure 7H). More excitingly, the necroptosis score was significantly higher in responders than in non-responders, as classified by the TIDE algorithm (<http://tide.dfci.harvard.edu/>) (Figure 7I). We next investigated whether the necroptosis signatures could predict patients' response to ICB therapy in real-world immunotherapy cohorts. Using four independent ICB cohorts comprising of four cancer types (Figure 7J), we found that patients with a response to ICB had consistently higher necroptosis score than patients with no response and that the high-necroptosis-score group presented a better response to ICB (Figure 7J, 7K). Hence, patients with a high necroptosis score tended to benefit more from treatment based on immune-checkpoint blockade (ICB).

## DISCUSSION

Necroptosis may prevent or promote the progression of tumor cells [36]. Höckendorf and colleagues identified RIPK3 as a key tumor suppressor in AML [15]. Paradoxically, high expression of RIPK3 leads to

productive proliferation and necrotic vulnerability in recurrent breast cancer [37]. Also, necroptosis-induced chemokine ligand 1 (CXCL1) expression may be crucial for the progression of pancreatic ductal adenocarcinoma and promote a macrophage-induced adaptive immune response [38]. Most studies have focused only on the effect of a single NRG or single TME cell type. Hence, we aimed to reveal the clinical characteristics and pattern of infiltration of TME cells mediated by multiple NRGs. Identifying the role of NRGs in the TME could provide important molecular insights into the interactions between necroptosis and the anti-tumor immune response, and facilitate development of more efficacious therapeutic strategies.

Sample classification is a widely applied method based on predefined gene sets. In the present study, 151 AML patients were classified into three subtypes according to expression of NRGs. Necroptosis cluster B carried a worse prognosis and was closely associated with immune system-related pathways, including “intestinal immune network for IgA production”, “NOD-like, and Toll-like receptor signaling pathway”, “B cell receptor signaling pathway”, and “natural killer cell-mediated cytotoxicity”. Simultaneously, the three necroptosis clusters differed significantly in terms of the characteristics of infiltration of immune cells. Based on the DEGs among the three necroptosis clusters, patients were classified into three gene clusters. Furthermore, on basis of the analysis stated above, we constructed a robust and effective necroptosis score to predict the response to clinical immunotherapy or patient survival. Patients with a low necroptosis score or high necroptosis score showed significant differences with regard to clinicopathological characteristics, prognosis, the TME, and immune checkpoints. Our findings suggest that NRGs might serve as a clinical predictive marker for evaluating the outcome and immunotherapy response of people suffering from AML.

The TME is crucial for understanding how cancer cells grow and progress, and has a vital role in tumor biology [39]. The TME comprises tumor-infiltrating immune cells (TIICs), fibroblasts, blood vessels, and the extracellular matrix [40]. Necroptosis induction is involved in the TME, and immunosuppression of the TME reduces the resistance of tumor cells to antitumor therapies [39]. Necroptosis-induced CXCL1 expression influences the immunosuppressive TME associated with intact RIP1/RIP3 signaling [38]. The association between the number of immune cells infiltrating and the clinical prognosis and treatment responsiveness has attracted attention recently. We showed that the relative abundance of 23 TIICs differed significantly except for CD56 bright natural killer cells between the three necroptosis clusters. Moreover, most immune cells were

positively related to the necroptosis score, which included activated dendritic cells, gamma delta T cells, macrophages, mast cells, and natural killer T cells. Gamma delta T cells has been reported to participate in regulating graft-versus-host disease and the graft-versus-leukemia effect [41, 42]. In addition, RIPK1 expression has been found to be upregulated in TAMs [43]. Also, inhibition of RIPK1-reprogrammed TAMs towards an immunogenic phenotype can elicit activation of cytotoxic T cells and differentiation of T-helper cells [43].

ICB therapy has shown promising clinical benefit in cancer (especially in solid tumors). Recently, immunotherapeutic drugs have been reported to lengthen survival in AML [44, 45]. Compared with their application in AML, immune-checkpoint inhibitors have provided more significant benefit in treatment of solid tumors such as melanoma and non-small-cell lung cancer [46, 47]. We wanted to identify novel molecular markers that could be used to screen AML patients and predict the response to immunotherapy precisely. We found higher expression of PD-1/PD-L1 and CD86 transcription in the group with a high necroptosis score with a poor prognosis. These data supported the potential predictive value of the necroptosis score on immunotherapy benefits. CTLA-4/CD80 and CD86 or PD-1/PD-L1 and PD-L2 participate in checkpoint control of T-cell effector functions, which can regulate T-cell activation [44]. Patients with malignant melanoma have been shown to achieve prolonged remission with the anti-CTLA-4 antibodies ipilimumab or tremelimumab [48]. We concluded that patients with a high necroptosis score, who had high expression of PD-1/PD-L1 and CD86, might respond to ICB. In addition, the necroptosis score was negatively associated with the TIDE score, MDSCs, and the M2 subtype of TAMs. The necroptosis score was positively related to IFNG, merck18, and T-cell dysfunction-score signatures. Patients with a high TIDE score are more likely to reduce the response to ICB treatment [49]. The TIDE score can help to identify patients that may be more likely to benefit from ICB [50]. The M2 subtype of TAMs contributes to immune suppression in the TME [51]. The necroptosis score was appreciably higher in responders than in non-responders. Patients with a high necroptosis score tended to benefit from ICB treatment. This finding might offer valuable insights into immunotherapy for AML patients.

While several other authors have also attempted to develop NRGs models for AML, we took a different approach to construct and validate a necroptosis score [52, 53]. There are also some limitations to this study. The prognostic model constructed for AML in this study needs to be further verified by large-

sample clinical studies. At the same time, although our bioinformatics analyses provided some immunological insights of NRGs in AML and highlighted their potential role as predictive biomarkers for immunotherapy, further investigations including prospective clinical assessment are required.

Therefore, we analyzed the NRG signature among 151 AML samples. We also evaluated the association of the NRG signature with the prognosis, clinicopathological features, and TME cell-infiltrating characteristics. Evaluating the NRG patterns of an individual tumor might provide important insights into “personalized” immunotherapy strategies for patients with AML.

## AUTHOR CONTRIBUTIONS

Jun Qian designed the research; Xiang-Mei Wen and Ji-Chun Ma organized and analyzed data; Zi-Jun Xu, Ye Jin, Xin-Yi Chen and Pei-Hui Xia prepared the figures and performed data analysis; Zi-Jun Xu, and Xiang-Mei Wen drafted the manuscript; Jiang Lin and Wei Qian polished and revised the article. All authors have read and approved the submitted version.

## ACKNOWLEDGMENTS

The authors would like to offer sincere gratitude to the reviewers for their constructive comments on this article.

## CONFLICTS OF INTEREST

The authors declare no conflicts of interest related to this study.

## FUNDING

This study was supported by the National Natural Science Foundation of China (81970118, 81900163), Medical Innovation Team of Jiangsu Province (CXTDB2017002), Zhenjiang Clinical Research Center of Hematology (SS2018009), Social Development Foundation of Zhenjiang (SH2022086, SH2019065, SH2021052), Scientific Research Project of The Fifth 169 Project of Zhenjiang (21), Scientific Research Project of The Sixth 169 Project of Zhenjiang (90, 445), Medical Education Collaborative Innovation Fund of Jiangsu University (JDY2023008, JDYY2023021).

## Editorial note

&This corresponding author has a verified history of publications using a personal email address for correspondence.

## REFERENCES

1. De Kouchkovsky I, Abdul-Hay M. 'Acute myeloid leukemia: a comprehensive review and 2016 update'. *Blood Cancer J.* 2016; 6:e441. <https://doi.org/10.1038/bcj.2016.50> PMID:27367478
2. Pei S, Pollyea DA, Gustafson A, Stevens BM, Minhajuddin M, Fu R, Riemondy KA, Gillen AE, Sheridan RM, Kim J, Costello JC, Amaya ML, Inguva A, et al. Monocytic Subclones Confer Resistance to Venetoclax-Based Therapy in Patients with Acute Myeloid Leukemia. *Cancer Discov.* 2020; 10:536–51. <https://doi.org/10.1158/2159-8290.CD-19-0710> PMID:31974170
3. Oki T, Mercier F, Kato H, Jung Y, McDonald TO, Spencer JA, Mazzola MC, van Gastel N, Lin CP, Michor F, Kitamura T, Scadden DT. Imaging dynamic mTORC1 pathway activity in vivo reveals marked shifts that support time-specific inhibitor therapy in AML. *Nat Commun.* 2021; 12:245. <https://doi.org/10.1038/s41467-020-20491-8> PMID:33431855
4. Vago L, Gojo I. Immune escape and immunotherapy of acute myeloid leukemia. *J Clin Invest.* 2020; 130:1552–64. <https://doi.org/10.1172/JCI129204> PMID:32235097
5. DeWolf S, Tallman MS. How I treat relapsed or refractory AML. *Blood.* 2020; 136:1023–32. <https://doi.org/10.1182/blood.2019001982> PMID:32518943
6. Lonetti A, Pession A, Masetti R. Targeted Therapies for Pediatric AML: Gaps and Perspective. *Front Pediatr.* 2019; 7:463. <https://doi.org/10.3389/fped.2019.00463> PMID:31803695
7. Degtarev A, Hitomi J, Germscheid M, Ch'en IL, Korkina O, Teng X, Abbott D, Cuny GD, Yuan C, Wagner G, Hedrick SM, Gerber SA, Lugovskoy A, Yuan J. Identification of RIP1 kinase as a specific cellular target of necrostatins. *Nat Chem Biol.* 2008; 4:313–21. <https://doi.org/10.1038/nchembio.83> PMID:18408713
8. Hitomi J, Christofferson DE, Ng A, Yao J, Degtarev A, Xavier RJ, Yuan J. Identification of a molecular signaling network that regulates a cellular necrotic cell death pathway. *Cell.* 2008; 135:1311–23. <https://doi.org/10.1016/j.cell.2008.10.044> PMID:19109899
9. Kearney CJ, Martin SJ. An Inflammatory Perspective on Necroptosis. *Mol Cell.* 2017; 65:965–73. <https://doi.org/10.1016/j.molcel.2017.02.024> PMID:28306512
10. Pasparakis M, Vandenabeele P. Necroptosis and its role in inflammation. *Nature.* 2015; 517:311–20. <https://doi.org/10.1038/nature14191> PMID:25592536
11. Galluzzi L, Vitale I, Abrams JM, Alnemri ES, Baehrecke EH, Blagosklonny MV, Dawson TM, Dawson VL, El-Deiry WS, Fulda S, Gottlieb E, Green DR, Hengartner MO, et al. Molecular definitions of cell death subroutines: recommendations of the Nomenclature Committee on Cell Death 2012. *Cell Death Differ.* 2012; 19:107–20. <https://doi.org/10.1038/cdd.2011.96> PMID:21760595
12. Najafav A, Chen H, Yuan J. Necroptosis and Cancer. *Trends Cancer.* 2017; 3:294–301. <https://doi.org/10.1016/j.trecan.2017.03.002> PMID:28451648
13. Liu ZG, Jiao D. Necroptosis, tumor necrosis and tumorigenesis. *Cell Stress.* 2019; 4:1–8. <https://doi.org/10.15698/cst2020.01.208> PMID:31922095
14. Thijssen R, Alvarez-Diaz S, Grace C, Gao MY, Segal DH, Xu Z, Strasser A, Huang DCS. Loss of RIPK3 does not impact MYC-driven lymphomagenesis or chemotherapeutic drug-induced killing of malignant lymphoma cells. *Cell Death Differ.* 2020; 27:2531–3. <https://doi.org/10.1038/s41418-020-0576-2> PMID:32555451
15. Höckendorf U, Yabal M, Herold T, Munkhbaatar E, Rott S, Jilg S, Kauschinger J, Magnani G, Reisinger F, Heuser M, Kreipe H, Sotlar K, Engleitner T, et al. RIPK3 Restricts Myeloid Leukemogenesis by Promoting Cell Death and Differentiation of Leukemia Initiating Cells. *Cancer Cell.* 2016; 30:75–91. <https://doi.org/10.1016/j.ccell.2016.06.002> PMID:27411587
16. Strilic B, Yang L, Albarrán-Juárez J, Wachsmuth L, Han K, Müller UC, Pasparakis M, Offermanns S. Tumour-cell-induced endothelial cell necroptosis via death receptor 6 promotes metastasis. *Nature.* 2016; 536:215–8. <https://doi.org/10.1038/nature19076> PMID:27487218
17. McCormick KD, Ghosh A, Trivedi S, Wang L, Coyne CB, Ferris RL, Sarkar SN. Innate immune signaling through differential RIPK1 expression promote tumor progression in head and neck squamous cell carcinoma. *Carcinogenesis.* 2016; 37:522–9. <https://doi.org/10.1093/carcin/bgw032> PMID:26992898

18. Chan FK, Luz NF, Moriwaki K. Programmed necrosis in the cross talk of cell death and inflammation. *Annu Rev Immunol.* 2015; 33:79–106.  
<https://doi.org/10.1146/annurev-immunol-032414-112248>  
PMID:[25493335](https://pubmed.ncbi.nlm.nih.gov/25493335/)
19. Jorgensen I, Rayamajhi M, Miao EA. Programmed cell death as a defence against infection. *Nat Rev Immunol.* 2017; 17:151–64.  
<https://doi.org/10.1038/nri.2016.147>  
PMID:[28138137](https://pubmed.ncbi.nlm.nih.gov/28138137/)
20. Zhu K, Liang W, Ma Z, Xu D, Cao S, Lu X, Liu N, Shan B, Qian L, Yuan J. Necroptosis promotes cell-autonomous activation of proinflammatory cytokine gene expression. *Cell Death Dis.* 2018; 9:500.  
<https://doi.org/10.1038/s41419-018-0524-y>  
PMID:[29703889](https://pubmed.ncbi.nlm.nih.gov/29703889/)
21. Orozco SL, Daniels BP, Yatim N, Messmer MN, Quarato G, Chen-Harris H, Cullen SP, Snyder AG, Ralli-Jain P, Frase S, Tait SWG, Green DR, Albert ML, Oberst A. RIPK3 Activation Leads to Cytokine Synthesis that Continues after Loss of Cell Membrane Integrity. *Cell Rep.* 2019; 28:2275–87.e5.  
<https://doi.org/10.1016/j.celrep.2019.07.077>  
PMID:[31461645](https://pubmed.ncbi.nlm.nih.gov/31461645/)
22. Yatim N, Jusforgues-Saklani H, Orozco S, Schulz O, Barreira da Silva R, Reis e Sousa C, Green DR, Oberst A, Albert ML. RIPK1 and NF- $\kappa$ B signaling in dying cells determines cross-priming of CD8<sup>+</sup> T cells. *Science.* 2015; 350:328–34.  
<https://doi.org/10.1126/science.aad0395>  
PMID:[26405229](https://pubmed.ncbi.nlm.nih.gov/26405229/)
23. Sprooten J, De Wijngaert P, Vanmeerbeek I, Martin S, Vangheluwe P, Schlenner S, Krysko DV, Parys JB, Bultynck G, Vandenabeele P, Garg AD. Necroptosis in Immuno-Oncology and Cancer Immunotherapy. *Cells.* 2020; 9:1823.  
<https://doi.org/10.3390/cells9081823>  
PMID:[32752206](https://pubmed.ncbi.nlm.nih.gov/32752206/)
24. Chen J, Wang H, Zhou L, Liu Z, Chen H, Tan X. A necroptosis-related gene signature for predicting prognosis, immune landscape, and drug sensitivity in hepatocellular carcinoma. *Cancer Med.* 2022; 11:5079–96.  
<https://doi.org/10.1002/cam4.4812>  
PMID:[35560794](https://pubmed.ncbi.nlm.nih.gov/35560794/)
25. He R, Zhang M, He L, Huang J, Man C, Wang X, Lang Y, Fan Y. Integrated Analysis of Necroptosis-Related Genes for Prognosis, Immune Microenvironment Infiltration, and Drug Sensitivity in Colon Cancer. *Front Med (Lausanne).* 2022; 9:845271.  
<https://doi.org/10.3389/fmed.2022.845271>  
PMID:[35479956](https://pubmed.ncbi.nlm.nih.gov/35479956/)
26. Nie S, Huili Y, He Y, Hu J, Kang S, Cao F. Identification of Bladder Cancer Subtypes Based on Necroptosis-Related Genes, Construction of a Prognostic Model. *Front Surg.* 2022; 9:860857.  
<https://doi.org/10.3389/fsurg.2022.860857>  
PMID:[35478725](https://pubmed.ncbi.nlm.nih.gov/35478725/)
27. Niu Z, Wang X, Xu Y, Li Y, Gong X, Zeng Q, Zhang B, Xi J, Pei X, Yue W, Han Y. Development and Validation of a Novel Survival Model for Cutaneous Melanoma Based on Necroptosis-Related Genes. *Front Oncol.* 2022; 12:852803.  
<https://doi.org/10.3389/fonc.2022.852803>  
PMID:[35387121](https://pubmed.ncbi.nlm.nih.gov/35387121/)
28. Shi H, Peng Q, Zhou X, He Y, Sun S. An Efficient Signature Based on Necroptosis-Related Genes for Prognosis of Patients With Pancreatic Cancer. *Front Genet.* 2022; 13:848747.  
<https://doi.org/10.3389/fgene.2022.848747>  
PMID:[35419022](https://pubmed.ncbi.nlm.nih.gov/35419022/)
29. Mayakonda A, Lin DC, Assenov Y, Plass C, Koeffler HP. Maftools: efficient and comprehensive analysis of somatic variants in cancer. *Genome Res.* 2018; 28:1747–56.  
<https://doi.org/10.1101/gr.239244.118>  
PMID:[30341162](https://pubmed.ncbi.nlm.nih.gov/30341162/)
30. Mermel CH, Schumacher SE, Hill B, Meyerson ML, Beroukhi R, Getz G. GISTIC2.0 facilitates sensitive and confident localization of the targets of focal somatic copy-number alteration in human cancers. *Genome Biol.* 2011; 12:R41.  
<https://doi.org/10.1186/gb-2011-12-4-r41>  
PMID:[21527027](https://pubmed.ncbi.nlm.nih.gov/21527027/)
31. Zhao Z, Liu H, Zhou X, Fang D, Ou X, Ye J, Peng J, Xu J. Necroptosis-Related lncRNAs: Predicting Prognosis and the Distinction between the Cold and Hot Tumors in Gastric Cancer. *J Oncol.* 2021; 2021:6718443.  
<https://doi.org/10.1155/2021/6718443>  
PMID:[34790235](https://pubmed.ncbi.nlm.nih.gov/34790235/)
32. Wilkerson MD, Hayes DN. ConsensusClusterPlus: a class discovery tool with confidence assessments and item tracking. *Bioinformatics.* 2010; 26:1572–3.  
<https://doi.org/10.1093/bioinformatics/btq170>  
PMID:[20427518](https://pubmed.ncbi.nlm.nih.gov/20427518/)
33. Zeng D, Li M, Zhou R, Zhang J, Sun H, Shi M, Bin J, Liao Y, Rao J, Liao W. Tumor Microenvironment Characterization in Gastric Cancer Identifies Prognostic and Immunotherapeutically Relevant Gene Signatures. *Cancer Immunol Res.* 2019; 7:737–50.  
<https://doi.org/10.1158/2326-6066.CIR-18-0436>  
PMID:[30842092](https://pubmed.ncbi.nlm.nih.gov/30842092/)
34. Newman AM, Liu CL, Green MR, Gentles AJ, Feng W, Xu Y, Hoang CD, Diehn M, Alizadeh AA. Robust

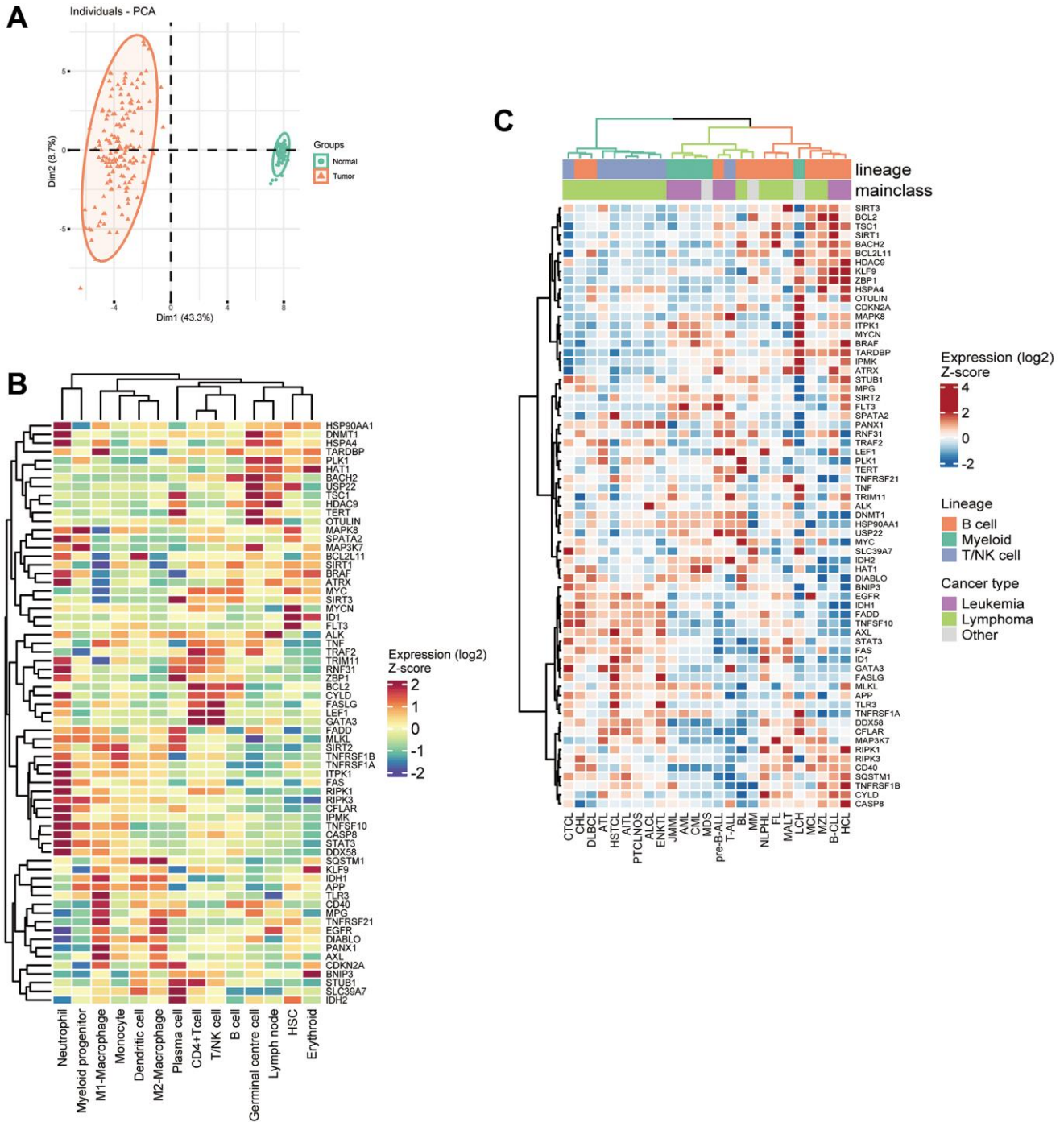
- enumeration of cell subsets from tissue expression profiles. *Nat Methods*. 2015; 12:453–7.  
<https://doi.org/10.1038/nmeth.3337>  
PMID:25822800
35. Yoshihara K, Shahmoradgoli M, Martínez E, Vegesna R, Kim H, Torres-Garcia W, Treviño V, Shen H, Laird PW, Levine DA, Carter SL, Getz G, Stemke-Hale K, et al. Inferring tumour purity and stromal and immune cell admixture from expression data. *Nat Commun*. 2013; 4:2612.  
<https://doi.org/10.1038/ncomms3612>  
PMID:24113773
36. Philipp S, Sosna J, Adam D. Cancer and necroptosis: friend or foe? *Cell Mol Life Sci*. 2016; 73:2183–93.  
<https://doi.org/10.1007/s00018-016-2193-2>  
PMID:27048810
37. Lin CC, Mabe NW, Lin YT, Yang WH, Tang X, Hong L, Sun T, Force J, Marks JR, Yao TP, Alvarez JV, Chi JT. RIPK3 upregulation confers robust proliferation and collateral cystine-dependence on breast cancer recurrence. *Cell Death Differ*. 2020; 27:2234–47.  
<https://doi.org/10.1038/s41418-020-0499-y>  
PMID:31988496
38. Seifert L, Werba G, Tiwari S, Gao Ly NN, Alothman S, Alqunaibit D, Avanzi A, Barilla R, Daley D, Greco SH, Torres-Hernandez A, Pergamo M, Ochi A, et al. The necrosome promotes pancreatic oncogenesis via CXCL1 and Mincle-induced immune suppression. *Nature*. 2016; 532:245–9.  
<https://doi.org/10.1038/nature17403>  
PMID:27049944
39. Siegel RL, Miller KD, Fuchs HE, Jemal A. Cancer Statistics, 2021. *CA Cancer J Clin*. 2021; 71:7–33.  
<https://doi.org/10.3322/caac.21654>  
PMID:33433946
40. Turley SJ, Cremasco V, Astarita JL. Immunological hallmarks of stromal cells in the tumour microenvironment. *Nat Rev Immunol*. 2015; 15:669–82.  
<https://doi.org/10.1038/nri3902>  
PMID:26471778
41. Fujishima N, Hirokawa M, Fujishima M, Yamashita J, Saitoh H, Ichikawa Y, Horiuchi T, Kawabata Y, Sawada KI. Skewed T cell receptor repertoire of Vdelta1(+) gammadelta T lymphocytes after human allogeneic haematopoietic stem cell transplantation and the potential role for Epstein-Barr virus-infected B cells in clonal restriction. *Clin Exp Immunol*. 2007; 149:70–9.  
<https://doi.org/10.1111/j.1365-2249.2007.03388.x>  
PMID:17425654
42. Godder KT, Henslee-Downey PJ, Mehta J, Park BS, Chiang KY, Abhyankar S, Lamb LS. Long term disease-free survival in acute leukemia patients recovering with increased gammadelta T cells after partially mismatched related donor bone marrow transplantation. *Bone Marrow Transplant*. 2007; 39:751–7.  
<https://doi.org/10.1038/sj.bmt.1705650>  
PMID:17450185
43. Wang W, Marinis JM, Beal AM, Savadkar S, Wu Y, Khan M, Taunk PS, Wu N, Su W, Wu J, Ahsan A, Kurz E, Chen T, et al. RIP1 Kinase Drives Macrophage-Mediated Adaptive Immune Tolerance in Pancreatic Cancer. *Cancer Cell*. 2018; 34:757–74.e7.  
<https://doi.org/10.1016/j.ccell.2018.10.006>  
PMID:30423296
44. Stamm H, Klingler F, Grossjohann EM, Muschhammer J, Vettorazzi E, Heuser M, Mock U, Thol F, Vohwinkel G, Latuske E, Bokemeyer C, Kischel R, Dos Santos C, et al. Immune checkpoints PVR and PVRL2 are prognostic markers in AML and their blockade represents a new therapeutic option. *Oncogene*. 2018; 37:5269–80.  
<https://doi.org/10.1038/s41388-018-0288-y>  
PMID:29855615
45. Hattori N, Kawaguchi Y, Sasaki Y, Shimada S, Murai S, Abe M, Baba Y, Watanuki M, Fujiwara S, Arai N, Kabasawa N, Tsukamoto H, Uto Y, et al. Monitoring TIGIT/DNAM-1 and PVR/PVRL2 Immune Checkpoint Expression Levels in Allogeneic Stem Cell Transplantation for Acute Myeloid Leukemia. *Biol Blood Marrow Transplant*. 2019; 25:861–7.  
<https://doi.org/10.1016/j.bbmt.2019.01.013>  
PMID:30639819
46. Alexandrov LB, Nik-Zainal S, Wedge DC, Aparicio SA, Behjati S, Biankin AV, Bignell GR, Bolli N, Borg A, Børresen-Dale AL, Boyault S, Burkhardt B, Butler AP, et al, and Australian Pancreatic Cancer Genome Initiative, and ICGC Breast Cancer Consortium, and ICGC MMML-Seq Consortium, and ICGC PedBrain. Signatures of mutational processes in human cancer. *Nature*. 2013; 500:415–21.  
<https://doi.org/10.1038/nature12477>  
PMID:23945592
47. Yarchoan M, Hopkins A, Jaffee EM. Tumor Mutational Burden and Response Rate to PD-1 Inhibition. *N Engl J Med*. 2017; 377:2500–1.  
<https://doi.org/10.1056/NEJMc1713444>  
PMID:29262275
48. Hodi FS, O'Day SJ, McDermott DF, Weber RW, Sosman JA, Haanen JB, Gonzalez R, Robert C, Schadendorf D, Hassel JC, Akerley W, van den Eertwegh AJ, Lutzky J, et al. Improved survival with ipilimumab in patients with metastatic melanoma. *N Engl J Med*. 2010; 363:711–23.  
<https://doi.org/10.1056/NEJMoa1003466>

PMID:[20525992](#)

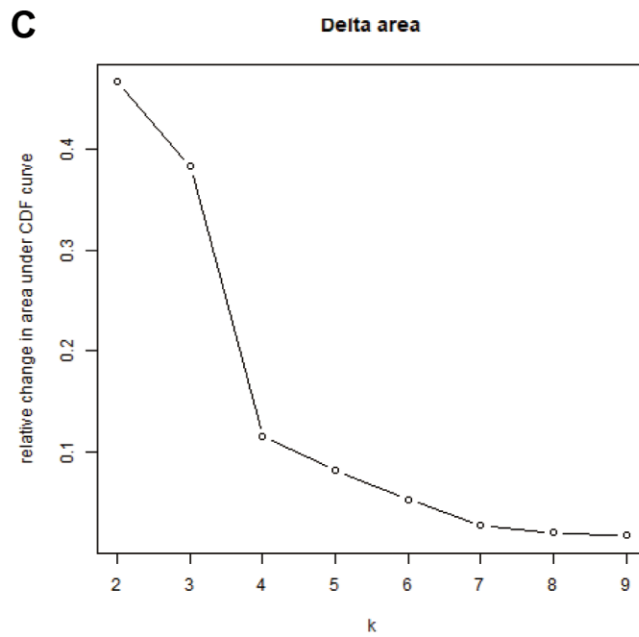
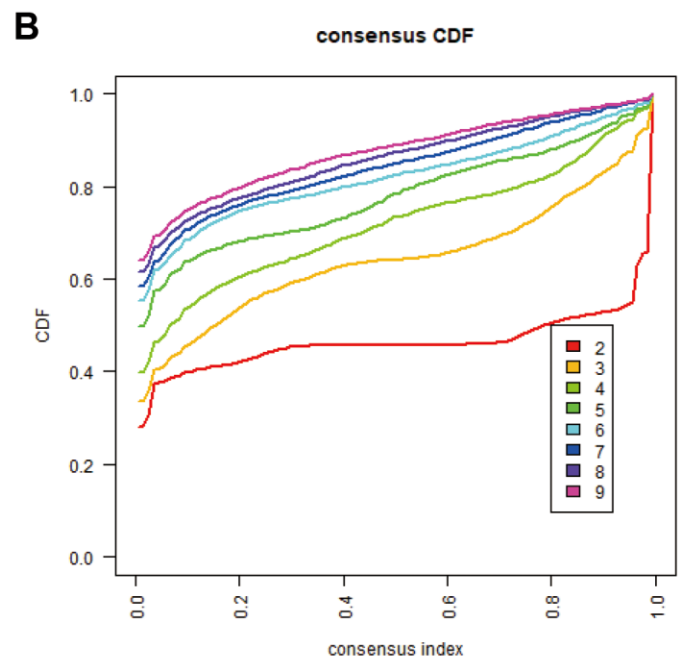
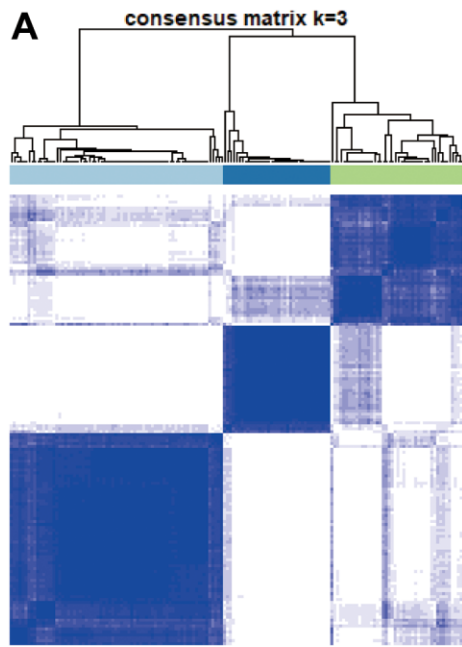
49. Wang Q, Li M, Yang M, Yang Y, Song F, Zhang W, Li X, Chen K. Analysis of immune-related signatures of lung adenocarcinoma identified two distinct subtypes: implications for immune checkpoint blockade therapy. *Aging* (Albany NY). 2020; 12:3312–39. <https://doi.org/10.18632/aging.102814> PMID:[32091408](#)
50. Jiang P, Gu S, Pan D, Fu J, Sahu A, Hu X, Li Z, Traugh N, Bu X, Li B, Liu J, Freeman GJ, Brown MA, et al. Signatures of T cell dysfunction and exclusion predict cancer immunotherapy response. *Nat Med*. 2018; 24:1550–8. <https://doi.org/10.1038/s41591-018-0136-1> PMID:[30127393](#)
51. Cassetta L, Fragkogianni S, Sims AH, Swierczak A, Forrester LM, Zhang H, Soong DYH, Cotechini T, Anur P, Lin EY, Fidanza A, Lopez-Yrigoyen M, Millar MR, et al. Human Tumor-Associated Macrophage and Monocyte Transcriptional Landscapes Reveal Cancer-Specific Reprogramming, Biomarkers, and Therapeutic Targets. *Cancer Cell*. 2019; 35:588–602.e10. <https://doi.org/10.1016/j.ccell.2019.02.009> PMID:[30930117](#)
52. Sun Y, Wang R, Xie S, Wang Y, Liu H. A Novel Identified Necroptosis-Related Risk Signature for Prognosis Prediction and Immune Infiltration Indication in Acute Myeloid Leukemia Patients. *Genes* (Basel). 2022; 13:1837. <https://doi.org/10.3390/genes13101837> PMID:[36292722](#)
53. Ma J, Jin Y, Gong B, Li L, Zhao Q. Pan-cancer analysis of necroptosis-related gene signature for the identification of prognosis and immune significance. *Discov Oncol*. 2022; 13:17. <https://doi.org/10.1007/s12672-022-00477-2> PMID:[35312867](#)

SUPPLEMENTARY MATERIALS

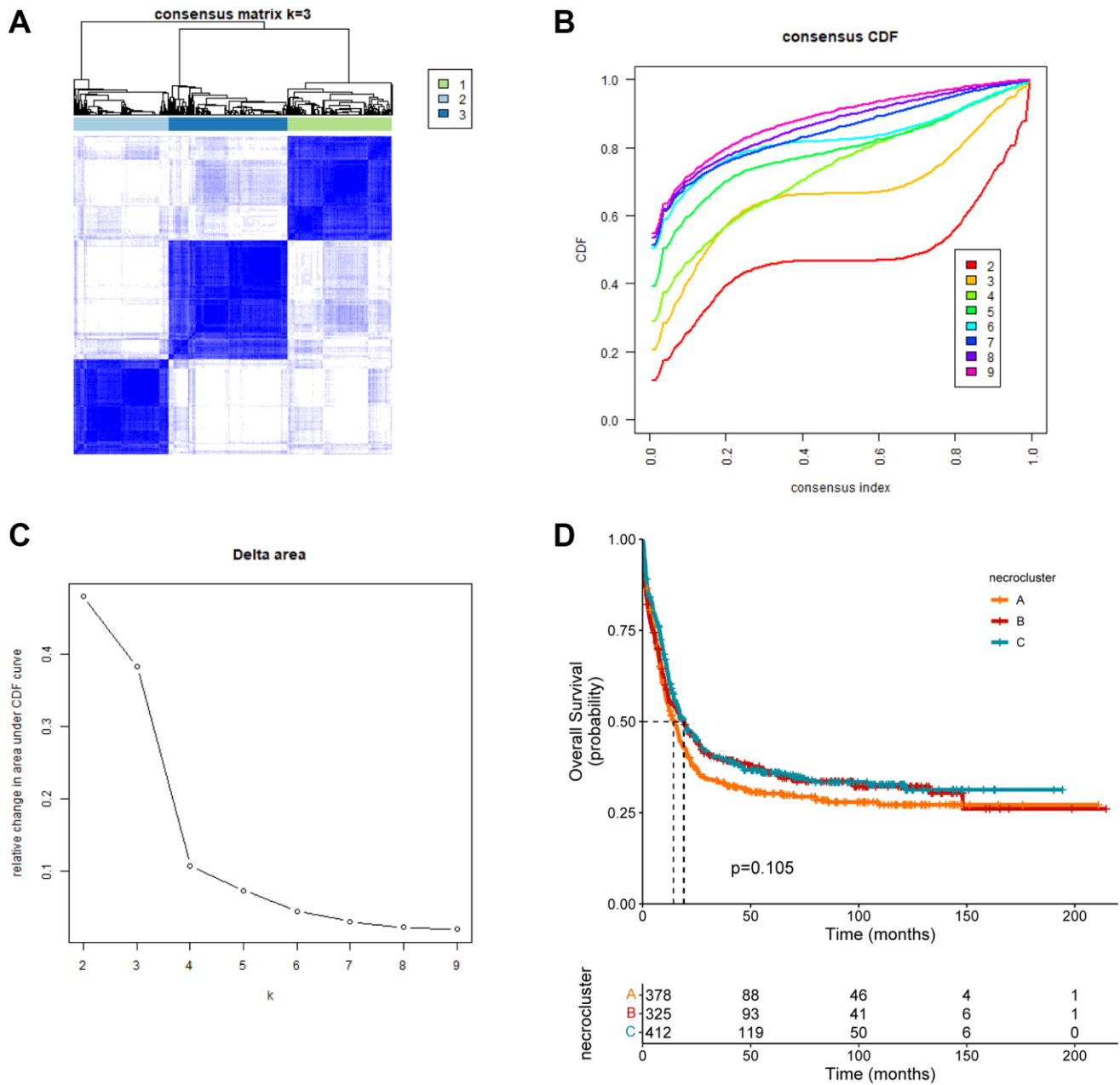
Supplementary Figures



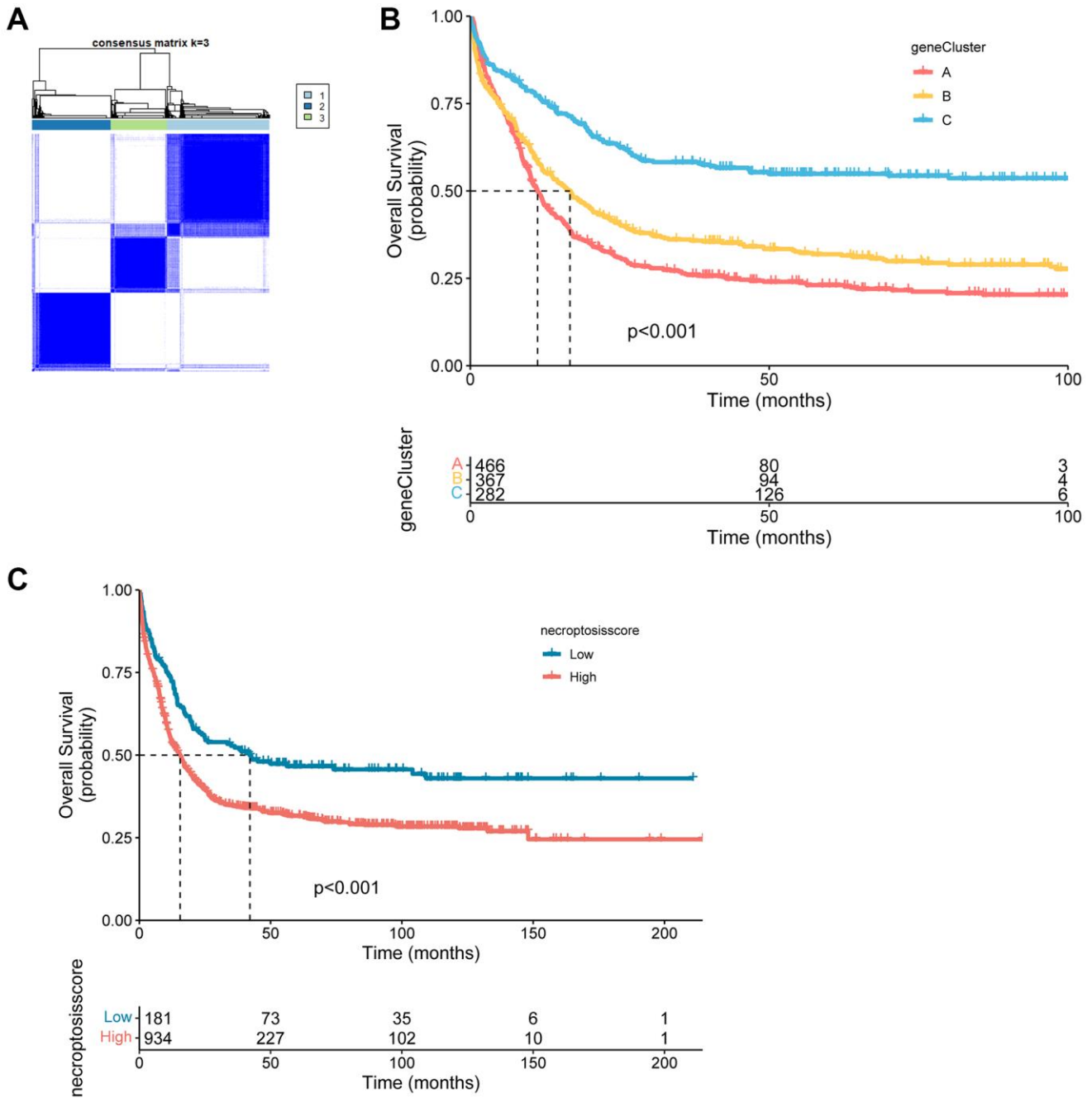
**Supplementary Figure 1. Characterization of necroptosis-related genes.** (A) Principal component analysis of 67 necroptosis-related genes based on paired tumor samples and normal samples. (B, C) Heatmap of expression of 67 necroptosis-related genes in different types of immune cells (B) and hematological malignancies (C).



**Supplementary Figure 2. Unsupervised clustering analyses of a necroptosis signature.** (A) Concordance matrix of subtypes. (B, C) Cumulative distribution function presented as the relative change in area when k = 2–9.



**Supplementary Figure 3. Consensus clustering analysis in combined AML cohorts encompassing six datasets (1115 patients).** (A) The concordance matrix of the subtypes was calculated. (B, C) The cumulative distribution function and relative change in area under the cumulative distribution function curve for  $k = 2-9$ . (D) Kaplan-Meier curves showing the overall survival for three clusters ( $P = 0.105$ , log-rank test).



**Supplementary Figure 4. Prognosis analysis of three gene clusters and the necroptosis score in combined AML cohorts encompassing six datasets (1115 patients).** (A) Consensus matrix heatmap defining three gene clusters ( $k = 3$ ). (B) Kaplan-Meier overall survival curves of three gene clusters ( $P < 0.001$ , log-rank test). (C) Kaplan-Meier survival analysis of high versus low necroptosis score groups ( $P < 0.001$ , log-rank test).

## Supplementary Tables

Please browse Full Text version to see the data of Supplementary Tables 1, 2, 5, 7–12 and 14.

**Supplementary Table 1. A total of 67 necroptosis-related genes in the study.**

**Supplementary Table 2. The copy number variation (CNV) of 67 necroptosis-related genes explored in AML.**

**Supplementary Table 3. The locations of 67 necroptosis-related genes on their respective chromosomes.**

Chromosome	chromStart	chromEnd	Gene
chr1	11012344	11026420	TARDBP
chr1	12167003	12209228	TNFRSF1B
chr1	172659018	172666874	FASLG
chr1	228393673	228406840	TRIM11
chr2	15940564	15947007	MYCN
chr2	29192774	29921566	ALK
chr2	111119378	111168447	BCL2L1
chr2	171922448	171983682	HAT1
chr2	201116104	201176687	CFLAR
chr2	201233443	201287711	CASP8
chr2	208236227	208266074	IDH1
chr3	172505508	172523507	TNFSF10
chr4	108047545	108168956	LEF1
chr4	186069152	186088069	TLR3
chr5	1253147	1295069	TERT
chr5	14664664	14699711	OTULIN
chr5	133051962	133106449	HSPA4
chr5	179806398	179838078	SQSTM1
chr6	3063991	3115187	RIPK1
chr6	31575567	31578336	TNF
chr6	33200445	33204439	SLC39A7
chr6	47231532	47309905	TNFRSF21
chr6	89926529	90296908	BACH2
chr6	90513573	90587045	MAP3K7
chr7	18086949	19002416	HDAC9
chr7	55019021	55256620	EGFR
chr7	140719327	140924764	BRAF
chrX	77504878	77786269	ATRX
chr8	127735434	127741434	MYC
chr9	21967753	21995301	CDKN2A
chr9	32455705	32526324	DDX58
chr9	70384597	70414624	KLF9
chr9	132891348	132944633	TSC1
chr9	136881912	136926607	TRAF2
chr11	215458	236931	SIRT3

chr11	70203163	70207390	FADD
chr11	94128928	94181972	PANX1
chr10	8053604	8075198	GATA3
chr10	48306639	48439360	MAPK8
chr10	58191517	58267934	IPMK
chr10	67884669	67918390	SIRT1
chr10	88990531	89015785	FAS
chr10	131966455	131982013	BNIP3
chr12	6328757	6342114	TNFRSF1A
chr12	122207662	122227534	DIABLO
chr13	28003274	28100592	FLT3
chr14	24146683	24160661	RNF31
chr14	24336021	24340045	RIPK3
chr14	92936914	93116320	ITPK1
chr14	102080738	102139699	HSP90AA1
chr15	90083045	90102504	IDH2
chr16	77007	85853	MPG
chr16	680224	682870	STUB1
chr16	23677656	23690367	PLK1
chr16	50742050	50801935	CYLD
chr16	74671855	74700960	MLKL
chr17	20999593	21043760	USP22
chr17	42313324	42388568	STAT3
chr18	63123346	63320128	BCL2
chr20	31605283	31606515	ID1
chr20	46118272	46129863	CD40
chr20	49903391	49915508	SPATA2
chr20	57603846	57620576	ZBP1
chr19	10133345	10231286	DNMT1
chr19	38878555	38899862	SIRT2
chr19	41219203	41261766	AXL
chr21	25880550	26171128	APP

**Supplementary Table 4. The CNV alterations of 67 necroptosis-related genes on their respective chromosomes.**

chromosome	start	stop	seg.mean
chr1	11012344	11026420	1
chr1	12167003	12209228	1
chr1	172659018	172666874	0
chr1	228393673	228406840	1
chr2	15940564	15947007	0
chr2	29192774	29921566	0
chr2	111119378	111168447	0
chr2	171922448	171983682	0
chr2	201116104	201176687	-1
chr2	201233443	201287711	-1

chr2	208236227	208266074	0
chr3	172505508	172523507	0
chr4	108047545	108168956	0
chr4	186069152	186088069	0
chr5	1253147	1295069	0
chr5	14664664	14699711	0
chr5	133051962	133106449	-1
chr5	179806398	179838078	-1
chr6	3063991	3115187	0
chr6	31575567	31578336	0
chr6	33200445	33204439	0
chr6	47231532	47309905	0
chr6	89926529	90296908	0
chr6	90513573	90587045	0
chr7	18086949	19002416	-1
chr7	55019021	55256620	0
chr7	140719327	140924764	-1
chrX	77504878	77786269	0
chr8	127735434	127741434	1
chr9	21967753	21995301	-1
chr9	32455705	32526324	0
chr9	70384597	70414624	-1
chr9	132891348	132944633	1
chr9	136881912	136926607	1
chr11	215458	236931	0
chr11	70203163	70207390	1
chr11	94128928	94181972	1
chr10	8053604	8075198	0
chr10	48306639	48439360	0
chr10	58191517	58267934	0
chr10	67884669	67918390	0
chr10	88990531	89015785	0
chr10	131966455	131982013	0
chr12	6328757	6342114	0
chr12	122207662	122227534	0
chr13	28003274	28100592	-1
chr14	24146683	24160661	-1
chr14	24336021	24340045	-1
chr14	92936914	93116320	0
chr14	102080738	102139699	0
chr15	90083045	90102504	0
chr16	77007	85853	0
chr16	680224	682870	0
chr16	23677656	23690367	0
chr16	50742050	50801935	1

chr16	74671855	74700960	-1
chr17	20999593	21043760	0
chr17	42313324	42388568	-1
chr18	63123346	63320128	0
chr20	31605283	31606515	1
chr20	46118272	46129863	-1
chr20	49903391	49915508	-1
chr20	57603846	57620576	1
chr19	10133345	10231286	1
chr19	38878555	38899862	1
chr19	41219203	41261766	1
chr21	25880550	26171128	-1

**Supplementary Table 5. Clinical information for 151 patients with AML.**

**Supplementary Table 6. The results of univariate Cox regression analysis of 67 necroptosis-related genes in AML.**

ID	HR	HR.95L	HR.95H	P-value	km
SIRT1	0.653185005	0.378242712	1.127981155	0.126532966	0.0141689
SIRT2	2.184984848	1.310189482	3.643868962	0.00274144	0.000156203
IPMK	0.832128264	0.576823465	1.200432177	0.325662055	0.114827499
FLT3	1.145843585	0.941964664	1.39385008	0.173235112	0.005395313
DDX58	1.078687703	0.714994691	1.627378742	0.718089398	0.089256771
AXL	0.893148058	0.616525233	1.293886138	0.550144066	0.003022712
HAT1	1.879445439	1.059558298	3.333761968	0.030942926	0.002192668
TRIM11	1.692538231	0.908277659	3.1539757	0.097514088	0.01034464
MYC	0.991110343	0.817531286	1.201543879	0.927573176	0.164023709
PLK1	0.978689975	0.754347237	1.269752204	0.871185873	0.02396733
MPG	1.377101107	0.988070387	1.919304011	0.058877071	0.000623289
TNFRSF1B	1.163894293	1.030802172	1.314170617	0.014301022	0.002521854
CASP8	1.300459795	0.701888456	2.409493508	0.403741253	0.148505378
RNF31	1.311566439	0.7462553	2.305117998	0.345845229	0.142074969
TSC1	0.865754449	0.518796244	1.444749792	0.581131898	0.003174917
PANX1	1.781511256	1.21093007	2.620946026	0.003372425	0.003850982
TLR3	0.768912602	0.442353635	1.336547374	0.351558403	0.103295508
DIABLO	0.448302915	0.191224639	1.050991677	0.064956574	0.00054681
EGFR	0.162124498	0.009434344	2.786028751	0.209898964	0.002225816
MYCN	0.900484343	0.792057853	1.023753566	0.109303252	0.03588317
SLC39A7	0.828131159	0.477791165	1.435357676	0.501561935	0.017329371
FAS	0.885475167	0.594179178	1.319578841	0.55013449	0.029230075
SQSTM1	1.135111031	0.772580721	1.66775719	0.518550154	0.015239662
BACH2	1.133161573	0.874854048	1.467736424	0.343599343	0.040783794
ATRX	0.916901721	0.617217044	1.362095836	0.66746871	0.198735659
HDAC9	1.155183906	0.95236621	1.40119404	0.14305802	0.002137129

ZBP1	1.68624203	1.124616735	2.52833885	0.011463859	0.001224679
MAPK8	0.697286568	0.417564651	1.164391087	0.16814127	0.223565352
BNIP3	0.577742784	0.381540903	0.874838641	0.009552699	0.003061902
RIPK1	1.045134946	0.493019116	2.215547064	0.908319629	0.044349595
ALK	2.600097719	0.8630238	7.833512993	0.08947663	0.001249055
BCL2L11	1.468472638	1.126975312	1.913450868	0.004439423	0.002552374
BRAF	0.480067011	0.27963122	0.824172405	0.007785274	0.001083898
HSPA4	1.301501392	0.809385541	2.092829423	0.276884707	0.006134598
TERT	1.32265337	0.953263779	1.83518138	0.094224722	0.001181906
MLKL	1.043130146	0.728780155	1.49307098	0.817482411	0.149133862
BCL2	0.823515447	0.640900027	1.058164554	0.129018388	0.007601644
ITPK1	1.897746809	1.33293067	2.701898179	0.000379003	1.31422E-05
CYLD	1.445531804	0.814540202	2.565327272	0.208012226	0.015127248
DNMT1	1.519224994	0.89849651	2.568785251	0.118627464	0.001731079
FADD	2.752830445	1.553552027	4.877902591	0.000521882	1.1015E-07
TNF	0.878746969	0.738113019	1.046176149	0.146321965	0.009964063
KLF9	1.296480875	1.068129904	1.573650033	0.008621241	0.001611377
IDH2	1.259520778	0.806763049	1.966367439	0.310013134	0.099546954
TRAF2	1.056712493	0.638818732	1.74797832	0.829909929	0.036640337
HSP90AA1	1.316781385	0.903432252	1.919250958	0.15224634	0.007182229
RIPK3	1.420721389	1.033504631	1.953014245	0.030545089	0.001200498
FASLG	1.041890084	0.639615345	1.697168392	0.869069192	0.028144583
CD40	1.206387454	0.932591082	1.560566809	0.153119006	0.000667904
SPATA2	0.746521175	0.406950179	1.369440027	0.344998987	0.055968205
ID1	1.200475632	1.006408247	1.431965354	0.042258402	0.000194623
LEF1	0.917595921	0.749311916	1.12367394	0.405440668	0.012767755
GATA3	1.015865859	0.786799863	1.31162128	0.903895127	0.06558502
CDKN2A	1.081608681	0.843680642	1.386635276	0.535970717	0.002878496
STAT3	0.683169486	0.389810292	1.197301752	0.183207074	0.030650878
TNFRSF21	1.106554528	0.929281323	1.317645037	0.25569587	0.076153834
IDH1	1.42470344	1.011777604	2.006152228	0.0426608	0.000541714
CFLAR	0.941588305	0.597826846	1.48301894	0.795109628	0.217209513
SIRT3	0.839786189	0.481646278	1.464229821	0.538170095	0.048744659
MAP3K7	1.055232867	0.516374652	2.156411823	0.882787486	0.084903579
TARDBP	1.462416141	0.705296405	3.032286788	0.306980494	0.033807403
APP	0.912122011	0.828108786	1.004658539	0.062084379	0.000465397
TNFSF10	1.015918702	0.860748485	1.199062012	0.851850785	0.162765083
OTULIN	0.765242099	0.427404261	1.370120806	0.36793924	0.051735805
TNFRSF1A	0.811636879	0.482530203	1.365208682	0.431505516	0.07905431
USP22	0.997466291	0.578531952	1.719765	0.992716961	0.241687143
STUB1	1.516106553	0.973929262	2.36010886	0.065332889	0.000233725

**Supplementary Table 7. The result of the GSEA enrichment analysis between necroptosis cluster A and necroptosis cluster B.**

**Supplementary Table 8. The result of the GSEA enrichment analysis between necroptosis cluster A and necroptosis cluster C.**

**Supplementary Table 9. The result of the GSEA enrichment analysis between m6A between necroptosis cluster B and necroptosis cluster C.**

**Supplementary Table 10. GO functional enrichment analyses of differentially expressed genes (DEGs).**

**Supplementary Table 11. 316 genes with  $p$ -value < 0.05 by univariate Cox regression analysis of 829 overlap genes.**

**Supplementary Table 12. Necroptosisscore that quantifies the necroptosis related genes signatures in 151 AML patients.**

**Supplementary Table 13. The univariate analyses of necroptosisscore in the TCGA.**

Beta	HR (95% CI for HR)	wald.test	P-value	variables
0.03893	1.04 (1.025–1.055)	26.96	2.074e-07	AGE
1.183	3.264 (2.175–4.898)	32.65	1.104e-08	AGEcat
0.005017	1.005 (1.001–1.009)	5.42	0.01995	WBC
0.2223	1.249 (0.8345–1.869)	1.17	0.28	WBCcat
0.146	1.157 (0.667–2.008)	0.27	0.6034	FLT3_n
–0.02775	0.9726 (0.4897–1.932)	0.01	0.9368	CEBPA
0.1453	1.156 (0.7373–1.813)	0.4	0.5269	NPM_n
1.63	5.105 (2.642–9.861)	23.55	1.219e-06	TP53
–0.2314	0.7934 (0.3846–1.637)	0.39	0.531	IDH1_n
0.01886	1.019 (0.5422–1.915)	0	0.9533	IDH2_n
0.6019	1.826 (1.159–2.876)	6.74	0.009435	DNMT3A
0.7677	2.155 (1.164–3.988)	5.98	0.01451	RUNX1
0.6329	1.883 (1.39–2.551)	16.71	4.344e-05	RISK
2.038	7.673 (2.424–24.29)	12.01	0.0005283	necroptosisscore_group
0.02592	1.026 (1.012–1.041)	12.74	0.000357	necroptosisscore

**Supplementary Table 14. Spearman analysis between immune cells and the necroptosisscore.**